

Published in final edited form as:

*J Am Chem Soc.* 2013 February 20; 135(7): 2825–2834. doi:10.1021/ja312523u.

## Temperature Independent Catalytic Two-Electron Reduction of Dioxygen by Ferrocenes with a Tris[2-(2-pyridyl)ethyl]amine-Copper(II) Catalyst in the Presence of Perchloric Acid

 Dipanwita Das<sup>†</sup>, Yong-Min Lee<sup>†</sup>, Kei Ohkubo<sup>‡</sup>, Wonwoo Nam<sup>\*,†</sup>, Kenneth D. Karlin<sup>\*,†,§</sup>, and Shunichi Fukuzumi<sup>\*,†,‡</sup>
<sup>†</sup>Department of Bioinspired Science, Ewha Womans University, Seoul 120-750, Korea

<sup>‡</sup>Department of Material and Life Science, Division of Advanced Science and Biotechnology, Graduate School of Engineering, ALCA (JST), Osaka University, Suita, Osaka 565-0871, Japan

<sup>§</sup>Department of Chemistry, The Johns Hopkins University, Baltimore, MD 21218, USA

### Abstract

Selective two-electron plus two-proton ( $2e^-/2H^+$ ) reduction of  $O_2$  to hydrogen peroxide by ferrocene (Fc) or 1,1'-dimethylferrocene ( $Me_2Fc$ ) in the presence of perchloric acid is catalyzed efficiently by a mononuclear copper(II) complex,  $[Cu^{II}(tepa)]^{2+}$  {tepa = tris[2-(2-pyridyl)ethyl]amine} (**1**) in acetone. The  $E_{1/2}$  value for  $[Cu^{II}(tepa)]^{2+}$  as measured by cyclic voltammetry is 0.07 V vs  $Fc/Fc^+$  in acetone, being significantly positive, which makes it possible to use relatively weak one-electron reductants such as Fc and  $Me_2Fc$  for the overall two-electron reduction of  $O_2$ . Fast electron transfer from Fc or  $Me_2Fc$  to **1** affords the corresponding  $Cu^I$  complex,  $[Cu^I(tepa)]^+$  (**2**), which reacts at low temperature (193 K) with  $O_2$ , however only in presence of  $HClO_4$  to afford the hydroperoxo complex,  $[Cu^{II}(tepa)(OOH)]^{2+}$  (**3**). The detailed kinetic study on the homogeneous catalytic system reveals the rate-determining step to be the  $O_2$ -binding process in the presence of  $HClO_4$  at lower temperature as well as at room temperature. The  $O_2$ -binding kinetics in the presence of  $HClO_4$  were studied, demonstrating that the rate of formation of the hydroperoxo complex (**3**) as well as the overall catalytic reaction remained virtually the same with changing temperature. The apparent lack of an activation energy for the catalytic two-electron reduction of  $O_2$  is shown to result from the existence of a pre-equilibrium between **2** and  $O_2$  prior to the formation of the hydroperoxo complex **3**. No further reduction of  $[Cu^{II}(tepa)(OOH)]^{2+}$  (**3**) by Fc or  $Me_2Fc$  occurred, and instead **3** is protonated by  $HClO_4$  to yield  $H_2O_2$  accompanied by regeneration of **1**, thus completing the catalytic cycle for the two-electron reduction of  $O_2$  by Fc or  $Me_2Fc$ .

### Introduction

Among copper proteins containing one or more copper ions as active site prosthetic groups, many are involved in dioxygen ( $O_2$ ) processing and they can be classified into several types depending on their function and their specific copper ion coordination environments.<sup>1,2</sup> Suitable ligation of the reduced form  $Cu^I$  complexes includes N-, S- or O-atom donor elements which at some point in the protein catalytic cycle allows for reaction with  $O_2$  to generate copper- $O_2$  complexes,  $Cu^{II}_n(O_2)$  ( $n$  = typically 1-3), which are utilized for  $O_2$ -

\*Corresponding Author: fukuzumi@chem.eng.osaka-u.ac.jp; karlin@jhu.edu; wwnam@ewha.ac.kr.

#### ASSOCIATED CONTENT

Supporting Information. Kinetic analyses (Figures S1 – S20) and full author list for ref 40. This material is available free of charge via the Internet at <http://pubs.acs.org>.

transport ( $2\text{Cu}^{\text{I}} + \text{O}_2 \leftrightarrow \text{Cu}_2(\text{O}_2)$ ) and substrate oxygenation.<sup>1-4</sup> Galactose oxidases<sup>5</sup> and amine oxidases,<sup>6</sup> which are one class of copper oxidases, catalyze two-electron substrate oxidations, while reducing  $\text{O}_2$  to hydrogen peroxide ( $\text{H}_2\text{O}_2$ ).<sup>7</sup> Multicopper oxidases such as laccase also activate oxygen at a site containing a three-plus-one arrangement of four Cu atoms, exhibiting remarkable electroactivity for the four-electron reduction of oxygen at potentials approaching the thermodynamic value of 1.2 V (vs RHE).<sup>8</sup> Cytochrome c oxidases (C<sub>c</sub>Os), with a bimetallic active site consisting of a heme a and Cu (Fe<sub>a3</sub>/Cu<sub>B</sub>) are also capable of catalyzing the four-electron reduction of dioxygen to water while coupling this process to membrane proton translocation and eventually to ATP biosynthesis.<sup>9,10</sup>

The catalytic four-electron reduction of dioxygen ( $\text{O}_2$ ) to water has merited increasing attention because not only to aid the elucidation of fundamental principles relevant to biological processes (as above), but also due to the technological significance such as in fuel cell applications.<sup>11-18</sup> In the fuel cell, the four-electron reduction of  $\text{O}_2$  is catalyzed at the cathode by platinum impregnated in carbon.<sup>19,20</sup> The high loadings of this precious metal that are required to achieve appreciable activity have prompted considerable activity in the development of catalysts based on non-precious metals such as Co, Cu and Fe.<sup>21-27</sup>

The catalytic two-electron reduction of  $\text{O}_2$  to  $\text{H}_2\text{O}_2$  has also attracted considerable interest, because  $\text{H}_2\text{O}_2$  has been regarded as a promising candidate as a sustainable and clean energy carrier.<sup>28-30</sup> The free enthalpy change of the decomposition of hydrogen peroxide producing  $\text{H}_2\text{O}$  and  $\text{O}_2$  is as large as  $-211 \text{ kJ mol}^{-1}$ .<sup>31</sup>  $\text{H}_2\text{O}_2$  has also been used as a highly efficient and environmentally benign oxidant in terms of delignification efficiency and the reduction of negative ecological impacts.<sup>32,33</sup>

With regard to copper complex catalysts for  $\text{O}_2$  reduction,<sup>17</sup> two mononuclear copper complexes having tmpa or bzpy1 ligands (tmpa = tris(2-pyridylmethyl)amine),<sup>24a</sup> BzPY1 = *N,N*-bis[2-(2-pyridyl)ethyl]benzylamine)<sup>24b</sup> and one dinuclear copper complex with N3 ligand (N3 = -(CH<sub>2</sub>)<sub>3</sub>-linked bis[(2-(2-pyridyl)ethyl)amine])<sup>24b</sup> (Scheme 1) have so far been found to efficiently catalyze four-electron reduction of  $\text{O}_2$  via the formation of  $[(\text{TMPA})\text{Cu}^{\text{II}}]_2(\mu\text{-}1,2\text{-O}_2^{2-})^{2+}$ ,  $[\text{Cu}^{\text{II}}_2(\text{BzPY}1)(\mu\text{-}(\text{O}^{2-})_2)^{2+}$  and  $[\text{Cu}^{\text{II}}_2(\text{N}3)(\mu\text{-}\eta^2\text{-O}_2^{2-})]^{2+}$  intermediates, respectively. These Cu- $\text{O}_2$  complexes were prone to reductive O-O bond cleavage with protons to give water, in preference to the protonation leading to  $\text{H}_2\text{O}_2$ .<sup>24</sup> By contrast, a binuclear Cu(II) complex  $[\text{Cu}^{\text{II}}_2(\text{XYLO})(\text{OH})]^{2+}$  (Scheme 1) {where XYLO is a *m*-xylene-linked bis[(2-(2-pyridyl)ethyl)amine] dinucleating ligand with copper-bridging phenolate moiety} has been reported to catalyze the two-electron reduction of  $\text{O}_2$  in the presence of trifluoroacetic acid via a hydroperoxo intermediate.<sup>26</sup> In all of these cases, however, a strong one-electron reductant such as decamethylferrocene (Fc\*) was required to reduce  $\text{O}_2$  with these Cu complex catalysts. In order to use weaker reductants, the one-electron reduction potentials of Cu<sup>II</sup> complexes should be more positive those found for  $[\text{Cu}^{\text{II}}_2(\text{XYLO})(\text{OH})]^{2+}$  ( $-0.67 \text{ V vs SCE}$ ).<sup>26</sup> However, Cu<sup>I</sup> complexes with rather positive one-electron oxidation potentials cannot react with  $\text{O}_2$ , as reported previously.<sup>34</sup> Thus, there has so far been no report on the selective two- or four-electron reduction of  $\text{O}_2$  by weaker one-electron reductants than Fc\* with Cu complexes.

We report herein the selective two-electron reduction of  $\text{O}_2$  by ferrocene (Fc) and 1,1'-dimethylferrocene (Me<sub>2</sub>Fc), which are much weaker one-electron reductants than Fc\*, using a mononuclear copper (II) complex,  $[\text{Cu}^{\text{II}}(\text{tepa})]^{2+}$  {tepa = tris[2-(2-pyridyl)ethyl]amine} (**1**) in the presence of  $\text{HClO}_4$  in acetone. This behavior is in sharp contrast to that observed for the analogous complex  $[\text{Cu}^{\text{II}}(\text{tmpa})]^{2+}$  {tmpa = tris[2-(2-pyridyl)methyl]amine}, which catalyzes the four-electron reduction of  $\text{O}_2$  to water rather than the two-electron reduction of  $\text{O}_2$  to  $\text{H}_2\text{O}_2$  in presence of  $\text{HClO}_4$  in acetone; there, a strong one-electron reductant was required.<sup>24a</sup> Thus, a difference of an additional one -CH<sub>2</sub>- (methylene group) in the

pyridylalkyl moiety of the ligand for Cu<sup>II</sup>, N(CH<sub>2</sub>CH<sub>2</sub>-py)<sub>2</sub> vs. N(CH<sub>2</sub>-py)<sub>2</sub> (py = 2-pyridyl), results in (i) a remarkable difference in terms of number of electrons by which molecular oxygen is reduced (two electrons vs four-electrons) and (ii) the reducing ability of one-electron reductants that can be employed to reduce O<sub>2</sub>. More surprisingly, the rate of catalytic two-electron reduction of O<sub>2</sub> by Me<sub>2</sub>Fc with **1** exhibits no temperature dependence. However, our study and analysis of the seemingly bizarre results suggesting there is no apparent activation energy for the catalytic reduction of O<sub>2</sub> can in fact be well understood. We have done this by clarifying the catalytic mechanism based on kinetic analyses as well as detection of the reactive intermediates involved in the catalytic cycle.

## Experimental Section

### Materials

Reagent grade quality solvents and chemicals were obtained commercially and used without further purification unless otherwise noted. 1,1'-dimethylferrocene (Me<sub>2</sub>Fc), ferrocene (Fc), hydrogen peroxide (30%) and HClO<sub>4</sub> (70%) were purchased from Aldrich Co., U.S., and NaI (99.5%) was from Junsei Chemical Co., Japan. Acetone was purchased from JT Baker, U.S., and used either without further purification for non-air-sensitive experiments. For air-sensitive experiments, acetone was dried and distilled under argon and then deoxygenated by bubbling with argon for 30–45 min and kept over activated molecular sieves (4 Å) in a glove box.<sup>35</sup> Preparation and handling of air-sensitive compounds were performed under an Ar atmosphere (<1 ppm O<sub>2</sub>, <1 ppm H<sub>2</sub>O) in a glovebox (Korea Kiyon Co., Ltd.). The copper complex [Cu<sup>II</sup>(tepa)](ClO<sub>4</sub>)<sub>2</sub> (**1**) (tepa = tris(2-(2-pyridyl)ethylamine)<sup>34</sup> was prepared according to the literature procedure.<sup>36</sup>

### Instrumentation

UV – vis spectra were recorded on a Hewlett-Packard 8453 diode array spectrophotometer equipped with a UNISOKU Scientific Instruments Cryostat USP-203A for low-temperature experiments or an UNISOKU RSP-601 stopped-flow spectrometer equipped with a MOS-type highly sensitive photodiode array. Cyclic voltammetry (CV) and differential pulse voltammetry (DPV) measurements were performed on an ALS 630B electrochemical analyzer, and voltammograms were measured in deaerated acetone containing 0.10 M tetra-*n*-butylammonium hexafluorophosphate (TBAPF<sub>6</sub>) as a supporting electrolyte at room temperature. A conventional three-electrode cell was used with a glassy carbon working electrode (surface area of 0.3 mm<sup>2</sup>), and a platinum wire was the counter electrode. The glassy carbon working electrode was routinely polished with a BAS polishing alumina suspension and rinsed with acetone before use. The potentials were measured with respect to the Ag/AgNO<sub>3</sub> (10 mM) reference electrode and were converted to values vs ferrocene/ferrocenium ion (Fc/Fc<sup>+</sup>). All electrochemical measurements were carried out under an atmospheric nitrogen pressure. X-band EPR spectra were recorded at 77 K using a JEOL JES-RE1XE spectrometer. The magnitude of modulation was chosen to optimize the resolution and signal-to-noise (S/N) ratio of the observed spectra under non-saturating microwave power conditions. The *g* values and hyperfine coupling constants were calibrated using an Mn<sup>2+</sup> marker. The experimental parameters for EPR spectra were as follows: microwave frequency = 9.2 GHz, microwave power = 1.0 mW and modulation frequency = 100 kHz. The EPR parameters were determined by anisotropic simulation using an AniSimu/FA version 2.0.0 program coded by JEOL Ltd.

### Kinetic Measurements

Spectral change in the UV–visible range were recorded on a Hewlett-Packard 8453 diode array spectrophotometer equipped with Unisoku thermostatted cell holder for low temperature experiments. Rate constants for oxidation reactions of ferrocene derivatives by

O<sub>2</sub> in the presence of catalytic amounts of [Cu<sup>II</sup>(tepa)]<sup>2+</sup> and an excess amount of perchloric acid (HClO<sub>4</sub>) in acetone at 298 K were determined by monitoring the appearance of the absorption band due to the corresponding ferrocenium ions (Fc<sup>+</sup>: λ<sub>max</sub> = 620 nm, ε<sub>max</sub> = 430 ± 20 M<sup>-1</sup> cm<sup>-1</sup>. Me<sub>2</sub>Fc<sup>+</sup>: λ<sub>max</sub> = 650 nm, ε<sub>max</sub> = 360 ± 20 M<sup>-1</sup> cm<sup>-1</sup>). The limiting concentration of O<sub>2</sub> in an acetone solution was prepared by a mixed gas flow of O<sub>2</sub> and Ar. The mixed gas controlled by using a gas mixer (SMTEK, Korea), which can mix O<sub>2</sub> and Ar gases at specific pressures and flow rates. The O<sub>2</sub> concentration in an O<sub>2</sub>-saturated acetone solution (11 mM) was previously determined by spectroscopic titration in the photooxidation of 10-methyl-9,10-dihydroacridine by O<sub>2</sub>.<sup>37</sup>

### Spectroscopic Measurements

The amount of H<sub>2</sub>O<sub>2</sub> produced in reactions was determined by titration with iodide ion.<sup>38</sup> The diluted acetone solution of the reduced product of O<sub>2</sub> was treated with an excess of NaI. The amount of I<sub>3</sub><sup>-</sup> formed was then quantified using its visible spectrum [λ<sub>max</sub> = 365 nm, ε = (2.5 ± 0.1) × 10<sup>4</sup> M<sup>-1</sup> cm<sup>-1</sup>].

### Low-Temperature Measurements

Under an open atmosphere, [Cu<sup>I</sup>(tepa)](ClO<sub>4</sub>)<sub>2</sub> (**1**) (0.16 × 10<sup>-3</sup> M) was dissolved in 3 mL of O<sub>2</sub>-free acetone. The cuvette was cooled to -80 °C in a Hewlett-Packard 8453 diode array spectrophotometer equipped with an Unisoku thermostatted cell holder. HClO<sub>4</sub> (3.0 × 10<sup>-3</sup> M) was added into the reaction solution, the formation of the hydroperoxo species was followed by the change in the absorbance at 345 nm (ε = 7000 ± 100 M<sup>-1</sup> cm<sup>-1</sup>) determined for [Cu<sup>II</sup>(tepa)(OOH)]<sup>+</sup>.

## Results and Discussion

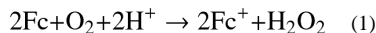
### Electrocatalytic Reduction of O<sub>2</sub> with [Cu<sup>II</sup>(tepa)](ClO<sub>4</sub>)<sub>2</sub> (**1**) in the Presence of HClO<sub>4</sub>

A cyclic voltammogram (CV) of **1** in deaerated acetone containing TBAPF<sub>6</sub> (0.10 M) at 298 K is shown in Figure 1. A quasi-reversible couple between the Cu<sup>II</sup> and Cu<sup>I</sup> forms of complex is observed. From the E<sub>1/2</sub> values, the one-electron reduction potentials (E<sub>red</sub>) of **1** was determined to be 0.07 ± 0.01 V (vs Fc/Fc<sup>+</sup>) (Figure 1, black line). The longer-armed tepa ligand, as compared to that observed in the tmpa ligand (Chart 1), leads to a complex **1** with coordination of a solvent (L), that is nearly perfectly square-based pyramidal in structure, results in nearly 0.5 V more positive shift of E<sub>red</sub> as compared with that of [Cu<sup>II</sup>(tmpa)]<sup>2+</sup> (**A**) (E<sub>red</sub> vs Fc/Fc<sup>+</sup> = -0.40 V).<sup>24a</sup> The tepa ligand forms six-membered chelates ring in **1**, whereas the tmpa ligand forms only five-membered chelate rings in [Cu<sup>II</sup>(tmpa)]<sup>2+</sup> (Chart 1). Such a change from the five to the six membered ring is generally known to result in a large positive shift in the Cu<sup>II/I</sup> redox potential.<sup>39</sup> This effect has its origin in the difference in ligand binding constants to Cu(II), which are much larger for five- vs six-membered chelate rings in multidentate ligands, as elucidated and summarized by Rorabacher and coworkers.<sup>39c,39d</sup>

The redox wave of the Cu<sup>II/I</sup> couple of **1** without HClO<sub>4</sub> in the presence of O<sub>2</sub> (red line in Figure 1) remains the same as that in the absence of O<sub>2</sub> (back line in Figure 1). In the presence of both O<sub>2</sub> and HClO<sub>4</sub>, however, a catalytic cathodic current is observed (blue line in Figure 1), indicating that O<sub>2</sub> can be reduced catalytically by **1** in the presence of HClO<sub>4</sub> in acetone. A slow sweep rate (1.0 mV s<sup>-1</sup>) is required to observed the catalytic cathodic current, indicating that the catalysis is a relatively slow process (vide infra).

### Catalytic Two-Electron Reduction of O<sub>2</sub> by Me<sub>2</sub>Fc and Fc with **1** in the Presence of HClO<sub>4</sub>

The addition of a catalytic amount of **1** to an acetone solution of Fc/Me<sub>2</sub>Fc containing O<sub>2</sub> ([O<sub>2</sub>] = 2.2 mM) and perchloric acid (HClO<sub>4</sub>) results in the efficient dioxygen reduction to afford the corresponding ferrocenium/dimethylferrocenium cation (Fc<sup>+</sup>/Me<sub>2</sub>Fc<sup>+</sup>) as shown in Figure 2 [see also Figure S1 in Supporting Information (SI)], where 2 equiv of Fc<sup>+</sup> (λ<sub>max</sub> = 620 nm) or Me<sub>2</sub>Fc<sup>+</sup> (λ<sub>max</sub> = 650 nm), relative to the number of mole equiv of O<sub>2</sub>, were formed in the presence of excess HClO<sub>4</sub>. Thus, the stoichiometry of the catalytic oxidation of Fc and Me<sub>2</sub>Fc by O<sub>2</sub> is given by eq 1. The formation of H<sub>2</sub>O<sub>2</sub> was confirmed by iodometric titration (Figure S2a in SI). The amount of I<sub>3</sub><sup>-</sup> produced (λ<sub>max</sub> = 365 nm) was the same as that produced by the reaction of the stoichiometric amount of H<sub>2</sub>O<sub>2</sub> with I<sup>-</sup> (Figure S2b in SI).



The rate of formation of Fc<sup>+</sup> and Me<sub>2</sub>Fc<sup>+</sup> obeyed pseudo-first order kinetics under the conditions that [**1**] ≪ [O<sub>2</sub>] ≪ [Me<sub>2</sub>Fc] ≪ [HClO<sub>4</sub>] (Figure 2 inset; Figure S1 inset in SI). Because two equiv of Fc<sup>+</sup> is formed in the reduction of O<sub>2</sub> (eq 1), the pseudo-first-order kinetics of formation of Fc<sup>+</sup> are given by eq 2, where the initial concentration of O<sub>2</sub> ([O<sub>2</sub>]<sub>0</sub>) is equal to two times of the final concentration of Fc<sup>+</sup> (2[Fc<sup>+</sup>]<sub>f</sub>); [Fc<sup>+</sup>] = 2{[O<sub>2</sub>]<sub>0</sub> - [O<sub>2</sub>]}. The time profiles of the absorbance at 620 nm

$$d[\text{Fc}^+] / dt = k_{\text{obs}} \left[ [\text{Fc}^+]_f - [\text{Fc}^+] \right] = k_{\text{obs}} [\text{O}_2] \quad (2)$$

due to Fc<sup>+</sup> and at 650 nm due to Me<sub>2</sub>Fc<sup>+</sup> and the first-order plots by varying catalyst (Figure 3a; see also Figures S4a, S5a and S5b in SI), HClO<sub>4</sub> (Figures S3a, S4b, S5c and S5d in SI), O<sub>2</sub> (Figures S3c, S4c, S6a and S6b in SI) and electron donors, Fc (Figures S3b and S4d in SI) and Me<sub>2</sub>Fc (Figures S6c and S6d in SI), are shown as indicated. The pseudo-first order rate constant (*k*<sub>obs</sub>) increased linearly with increasing concentration of **1** (Figure 3b; Figure S7a in SI), HClO<sub>4</sub> (Figure 4a; Figure S7b in SI) whereas the *k*<sub>obs</sub> value remains the same with increasing concentration of O<sub>2</sub> (Figures S3d and S7c in SI; note that the reaction rate is already first order with respect to [O<sub>2</sub>], cf eq 2), Fc (Figure 4b) and Me<sub>2</sub>Fc (Figures S7d in SI). Thus, the overall rate expression is given by eq 3, where *k*<sub>cat</sub> is the apparent third-order rate constant for the catalytic two-electron reduction of O<sub>2</sub> by Fc and Me<sub>2</sub>Fc. The kinetic formulation in eq 3 obtained in this study is quite unique because the rate

$$d[\text{Fc}^+] / dt = k_{\text{cat}} [\text{1}] [\text{O}_2] [\text{H}^+] \quad (3)$$

is proportional to concentrations of not only the catalyst **1** but also O<sub>2</sub> and HClO<sub>4</sub>. In such a case, the rate-determining step in the catalytic cycle should involve the reactions of **1** with O<sub>2</sub> and H<sup>+</sup>. In order to elucidate the catalytic mechanism that could explain such a unique kinetic formulation, we decided to examine each step in the catalytic cycle, step by step.

We also examined the overall catalytic reaction at different temperatures. Remarkably, variable temperature studies revealed that the catalytic rate was not affected by changes in temperature (Figure 5).

### Electron Transfer from Ferrocene Derivatives to **1**

Electron transfer from Fc and Me<sub>2</sub>Fc (*E*<sub>ox</sub> = 0.0 V and -0.11 V vs Fc/Fc<sup>+</sup>)<sup>40,41</sup> to **1** (*E*<sub>red</sub> = 0.07 V vs Fc/Fc<sup>+</sup>, vide supra) occurs efficiently because the reactions are exergonic (Δ*G*<sub>et</sub> < 0). The rates of electron transfer from Fc or Me<sub>2</sub>Fc to **1** were too fast to be determined at 298 K. Thus, these kinetics were determined at lower temperatures. The rate of formation of



Fc<sup>+</sup> and Me<sub>2</sub>Fc<sup>+</sup> obeyed pseudo-first-order kinetics in acetone at lower temperatures (see the time profiles in Figures 6a, S8a, S8c, S9a, S11a, S11c, S12a and S12c; first-order plots in Figures S8b, S8d, S9b, S10a, S11b, S11d, S12b and S12d in SI). The observed pseudo-first-order rate constant ( $k_{\text{obs}}$ ) increased linearly with increasing concentration of Fc and Me<sub>2</sub>Fc (Figure 6b; see also Figures S10 and S13 in SI). The second-order rate constant ( $k_{\text{et}}$ ) for electron transfer from Fc to **1** was determined from the slope of a linear plot of  $k_{\text{obs}}$  versus [Fc]. The temperature dependence of  $k_{\text{et}}$  was examined (Figure S14 in SI) and the second-order rate constant of electron transfer from Fc and Me<sub>2</sub>Fc to **1** at 298 K was determined to be  $(6.0 \pm 0.3) \times 10^4 \text{ M}^{-1} \text{ s}^{-1}$  and  $(6.1 \pm 0.3) \times 10^4 \text{ M}^{-1} \text{ s}^{-1}$ , respectively, from extrapolations of the Eyring plots (Figure S14 in SI). The  $k_{\text{et}}$  values for electron transfer from Fc or Me<sub>2</sub>Fc to **1** are significantly larger than the corresponding  $k_{\text{obs}}/[\mathbf{1}]$  (see eq 2) values ( $18 \pm 1 \text{ M}^{-1} \text{ s}^{-1}$  in Figure 3b for Fc and  $17 \pm 1 \text{ M}^{-1} \text{ s}^{-1}$  in Figure S7a for Me<sub>2</sub>Fc), respectively. Thus, it has been confirmed that the electron-transfer step is not the rate-determining step in the catalytic cycle, being consistent with the kinetic equation (eq 2), where the  $k_{\text{obs}}$  values were independent of the concentrations of [Fc] and [Me<sub>2</sub>Fc]. (Figures 4b and S7d).

The Eyring plot (Figure S14) affords the activation enthalpy ( $\Delta H = 9.5 \pm 0.2 \text{ kcal mol}^{-1}$  and  $9.2 \pm 0.2 \text{ kcal mol}^{-1}$ ) and activation entropy ( $\Delta S = -3 \pm 2 \text{ cal K}^{-1} \text{ mol}^{-1}$  and  $-2 \pm 2 \text{ cal K}^{-1} \text{ mol}^{-1}$ ) for Fc and Me<sub>2</sub>Fc reaction, respectively. An activation entropy close to zero was previously reported for electron transfer from ferrocene derivatives to Cu(II) complexes.<sup>26,42</sup> The electron transfer from Fc and Me<sub>2</sub>Fc to **1** results in formation of the Cu(I) complex, [Cu<sup>I</sup>(tepa)]<sup>+</sup> (**2**), which can reduce O<sub>2</sub> in presence of HClO<sub>4</sub>. Next we examined the reaction of [Cu<sup>I</sup>(tepa)]<sup>+</sup> with O<sub>2</sub> in presence of HClO<sub>4</sub> at low temperatures to detect intermediates.

### Detection of Intermediates in the Catalytic Two-Electron Reduction of O<sub>2</sub> by Fc with [Cu<sup>II</sup>(tepa)]<sup>2+</sup> (**1**)

When **1** was treated with O<sub>2</sub> and HClO<sub>4</sub>, a bright green colored hydroperoxo complex **3** (vide infra) was produced, possessing an intense absorption band at 345 nm ( $\epsilon = 7000 \pm 100 \text{ M}^{-1} \text{ cm}^{-1}$ ) corresponding to a LMCT band (HOO<sup>-</sup> → Cu), and a *d-d* transition envelope at 660 nm ( $\epsilon = 160 \pm 5 \text{ M}^{-1} \text{ cm}^{-1}$ ) (Figure 7).

The stoichiometry of O<sub>2</sub> binding step in presence of HClO<sub>4</sub> was determined by a control reaction. When Fc was used exactly at the level of one equiv relative to [Cu<sup>II</sup>(tepa)]<sup>2+</sup> (Figure S15), the amount of **3** produced is about one-half judging from a comparison of the results in Figure 7 with those in Figure S15. Thus, the stoichiometry of formation of **3** from the copper(I) complex is: [Cu<sup>I</sup>(tepa)]<sup>+</sup> + Fc + O<sub>2</sub> → [Cu<sup>II</sup>(tepa)(OOH)]<sup>+</sup> (**3**).

The formation of hydroperoxo complex was again checked by an alternative “authentic” method. Figure S16 shows the spectral change for the reaction of complex [Cu<sup>II</sup>(tepa)]<sup>2+</sup> (**1**) and H<sub>2</sub>O<sub>2</sub> (10 equiv) in acetone at 193 K in the presence of 2 equiv of Me<sub>4</sub>NOH. The result is that the same absorption band at 345 nm ( $\epsilon = 7000 \pm 100 \text{ M}^{-1} \text{ cm}^{-1}$ ) appears together with a *d-d* band at 660 nm ( $\epsilon = 160 \pm 5 \text{ M}^{-1} \text{ cm}^{-1}$ ) (see Figure S16).

It should be noted here that Masuda, Kodera and Itoh and their coworkers have reported on similar Cu(II)-hydroperoxo complexes with tridentate N<sub>3</sub> or tetradentate N<sub>4</sub> pyridylalkylamine ligands, such as the ligand bpba (bpba = bis(2-pyridylmethyl-*tert*-butylamine) which has a strong absorption band at 350 nm ( $\epsilon = 3400 \pm 100 \text{ M}^{-1} \text{ cm}^{-1}$ ) and *d-d* bands at 564 nm ( $\epsilon = 150 \pm 5 \text{ M}^{-1} \text{ cm}^{-1}$ ) and 790 (sh).<sup>43</sup> There were several other Cu(II)-hydroperoxo complexes reported hitherto having LMCT bands which lie in the highest energy region (380 nm for five-coordinate trigonal bipyramidal [Cu(bppa)(OOH)]<sup>+</sup> where bppa = bis(6-pivalamido-2-pyridylmethyl)(2-pyridylmethyl)amine,<sup>44</sup> 357 nm for five-coordinate square-pyramidal [Cu(N<sub>3</sub>S-type)(OOH)]<sup>+</sup> where N<sub>3</sub>S = 2-bis(6-methyl-2-

pyridylmethyl)amino-1-(phenylthio)-ethane,<sup>45</sup> 395 nm for five-coordinate  $[\text{Cu}^{\text{II}}_2(\text{XYL-O})-(\text{OOH})]^{2+}$  where  $\text{XYL-O} = 2,6\text{-bis}[\text{bis}[2\text{-(2-pyridyl)ethyl}]\text{-amino}]\text{phenolate}$ ,<sup>46</sup> and 379 nm for five-coordinate  $[\text{Cu}^{\text{II}}(\text{tmpa})(\text{OOH})]^+$  where  $\text{tmpa} = \text{tris}(2\text{-pyridylmethyl})\text{amine}$ .<sup>43,47</sup>

An EPR spectrum of  $[\text{Cu}^{\text{II}}(\text{tepa})]^{2+}$  in frozen acetone solution at 77 K exhibits the parameters,  $g_{\parallel} = 2.320 \pm 0.002$ ,  $g_{\perp} = 2.128 \pm 0.001$  and  $|A_{\parallel}| = 159 \pm 3$  G, indicating the typical tetragonal spectrum for four-lines in the downfield region due to Cu nuclear spin ( $I = 3/2$ ) (Figure 8a). The reaction of  $[\text{Cu}^{\text{I}}(\text{tepa})]^+$  (**2**), which was produced by the electron-transfer reduction of  $[\text{Cu}^{\text{II}}(\text{tepa})]^{2+}$  (**1**) by  $\text{Me}_2\text{Fc}$ , with  $\text{O}_2$  in the presence of  $\text{HClO}_4$  in acetone afforded an EPR spectrum at 77 K with EPR parameters of  $g_{\parallel} = 2.259 \pm 0.002$ ,  $g_{\perp} = 2.063 \pm 0.001$  and  $|A_{\parallel}| = 165 \pm 3$  G due to Cu with superhyperfine splitting due to three equivalent nitrogens ( $|A(3\text{N})_{\perp}| = 14.3 \pm 0.5$  G) as shown in Figure 8b. This spectrum is clearly different from that of  $[\text{Cu}^{\text{II}}(\text{tepa})]^{2+}$  (see Figure 8a) whereas the same EPR spectrum was observed at 77 K for  $[\text{Cu}^{\text{II}}(\text{tepa})\text{OOH}]^+$ , which was produced by the reaction of  $[\text{Cu}^{\text{II}}(\text{tepa})]^{2+}$  with  $\text{H}_2\text{O}_2$  in the presence of  $\text{Me}_4\text{NOH}$  in acetone. The computer simulated spectra of  $[\text{Cu}^{\text{II}}(\text{tepa})]^{2+}$  and  $[\text{Cu}^{\text{II}}(\text{tepa})\text{OOH}]^+$  with the EPR parameters described above agree perfectly with the observed spectra as shown in Figure 8.<sup>48</sup>

A similar EPR spectrum was reported for  $[\text{Cu}(\text{bpba})(\text{OOH})]^+$  with EPR parameters of  $g_{\parallel} = 2.26$ ,  $g_{\perp} = 2.06$  and  $|A_{\parallel}| = 175$  G in acetone at 77 K, although no superhyperfine due to nitrogens was observed in that case.<sup>43</sup> Thus, the EPR spectrum observed in Figure 8b together with the LMCT band seen in the higher energy region in Figure 7 strongly suggests the formation of  $[\text{Cu}^{\text{II}}(\text{tepa})\text{OOH}]^+$  in the reaction of  $[\text{Cu}^{\text{I}}(\text{tepa})]^+$  with  $\text{O}_2$  in the presence of  $\text{HClO}_4$  in acetone.

$[\text{Cu}^{\text{I}}(\text{tepa})]^+$  (**2**) was known to be unreactive towards  $\text{O}_2$  in the absence of  $\text{HClO}_4$ .<sup>34</sup> This lack of reactivity likely results from a combination of steric hindrance, electronic effects and also from the complex's high positive redox potential. The crystal structures of  $[\text{Cu}^{\text{II}}(\text{tepa})]^{2+}$  (**1**) and  $[\text{Cu}^{\text{I}}(\text{tepa})]^+$  were reported earlier.<sup>49,50</sup> The structural parameters clearly indicate that both the complexes are strongly constrained. Because the arm size of the *tepa* ligand is larger than *tmpa* ligand, any steric effects may be more prominent with *tepa*'s six membered chelate rings; the pyridyl rings of the donor ligands may extend out more into the region around the  $\text{Cu}^{\text{II}}$  ion where a fifth ligand, such as hydroperoxide anion, would approach and bind the metal ion.

In another homologous set of structures,  $[\text{Cu}^{\text{II}}(\text{tepa})\text{Cl}]^+$  and  $[\text{Cu}^{\text{II}}(\text{tmpa})\text{Cl}]^+$ , the  $\text{Cu}^{\text{II}}\text{-Cl}$  bond is also found to be lengthened in the *tepa* case, by  $0.056 \text{ \AA}$ .<sup>39a</sup> In fact, in all *tepa* vs. *tmpa*  $\text{Cu}^{\text{II}}$  pentacoordinate structures,  $[\text{Cu}^{\text{II}}(\text{tepa})\text{X}]^{2+/+}$ , the anionic or neutral X ligand is in an equatorial position of an overall square-based pyramidal structure, while the X-ligand in  $[\text{Cu}^{\text{II}}(\text{tmpa})\text{X}]^{2+/+}$  structures is in an axial position of a nearly perfect trigonal bipyramidal coordination environment.<sup>34,39a</sup> For  $[\text{Cu}^{\text{II}}(\text{tepa})\text{-OOH}]^+$ , due to (i) the hydroperoxo-ligand position in the coordination environment or (ii) because of a likely elongated Cu-O bond, (iii) or both, cleavage by acid to produce  $\text{H}_2\text{O}_2$  is preferred. This is in contrast to the O-O reductive cleavage which is observed for the intermediate  $[\text{Cu}^{\text{II}}(\text{tmpa})\text{OOH}]^+$  species likely formed during the four-electron four proton reduction of  $\text{O}_2$  to water using  $[\text{Cu}^{\text{II}}(\text{tmpa})]^{2+}$  as catalyst (vide infra).<sup>24a</sup>

The rate of formation of  $[\text{Cu}^{\text{II}}(\text{tepa})\text{OOH}]^+$  at 193 K obeyed first-order kinetics (Figures 9a and S17) and the pseudo-first-order rate constant increased in proportion to the concentration of  $\text{HClO}_4$  (Figure 9b). The observed rate constant exhibits no temperature dependence in the range between 193 and 223 K (Figures 10 and S18 in SI). The apparent zero activation energy or even negative activation energy has precedence and has been observed for reactions when an intermediate first forms and when the absolute value of the

heat of formation of the intermediate is equal to or larger than the activation enthalpy of the subsequent conversion of intermediate to the products, i.e.,  $-\Delta H \geq \Delta H^\ddagger$ .<sup>51-55</sup>

In the case of  $[\text{Cu}^{\text{I}}(\text{tmpa})]^+$ , the reaction of  $[\text{Cu}^{\text{I}}(\text{tmpa})]^+$  with  $\text{O}_2$  is known to produce the superoxo complex  $[\text{Cu}^{\text{II}}(\text{tmpa})(\text{O}_2^{\cdot-})]^+$ . The  $\Delta H$  and  $\Delta S$  values were reported to be  $-11 \text{ kcal mol}^{-1}$  and  $-23 \text{ cal K}^{-1} \text{ mol}^{-1}$ , respectively, when the  $\Delta G$  value at 193 K is  $-6.7 \text{ kcal mol}^{-1}$ .<sup>56</sup> This indicates the formation of the superoxo complex is highly exergonic. The formation of  $[\text{Cu}^{\text{II}}(\text{tmpa})(\text{O}_2^{\cdot-})]^+$  is followed by the reduction with another molecule of  $[\text{Cu}^{\text{I}}(\text{tmpa})]^+$  to produce the dinuclear copper(II)-peroxo (end-on) complex.<sup>56</sup>

In the case of  $[\text{Cu}^{\text{I}}(\text{tepa})]^+$ , neither a superoxo nor peroxo complex has been observed by the reaction with  $\text{O}_2$  at 193 K. Thus, the  $\Delta G$  value of formation of the superoxo complex,  $[\text{Cu}^{\text{II}}(\text{tepa})(\text{O}_2^{\cdot-})]^+$  must be positive. The activation barrier to access the superoxo complex in the absence of protons is too high. However, this does not necessarily mean that the  $\Delta H$  value is also positive. If the  $\Delta S$  value of formation of  $[\text{Cu}^{\text{II}}(\text{tepa})(\text{O}_2^{\cdot-})]^+$  is the same as that of  $[\text{Cu}^{\text{II}}(\text{tmpa})(\text{O}_2^{\cdot-})]^+$ , i.e., large and negative, the  $\Delta G$  value becomes positive (endergonic, therefore no formation) when the  $\Delta H$  value is more positive than  $-5.0 \text{ kcal mol}^{-1}$ .

Thus, the  $\Delta H$  value of formation of  $[\text{Cu}^{\text{II}}(\text{tepa})(\text{O}_2^{\cdot-})]^+$  could be negative enough to compensate for the  $\Delta H$  value required for the subsequent PCET reduction to produce the peroxo complex,  $[\text{Cu}^{\text{II}}(\text{tepa})\text{OOH}]^+$ , formation of which was observed at 193 K as shown in Figure 7. The energetics of formation of  $[\text{Cu}^{\text{II}}(\text{tepa})\text{OOH}]^+$  via the PCET reduction of  $[\text{Cu}^{\text{II}}(\text{tepa})(\text{O}_2^{\cdot-})]^+$  are shown in Scheme 2. If the  $-\Delta H$  value of formation of  $[\text{Cu}^{\text{II}}(\text{tepa})(\text{O}_2^{\cdot-})]^+$  happens to be equal or very close to the  $\Delta H$  value of PCET reduction of  $[\text{Cu}^{\text{II}}(\text{tepa})(\text{O}_2^{\cdot-})]^+$  (Scheme 2), the formation rate of  $[\text{Cu}^{\text{II}}(\text{tepa})\text{OOH}]^+$  would be independent of temperature as observed in this chemical system, see Figures 10 and S18 in SI.

No electron transfer from Fc or  $\text{Me}_2\text{Fc}$  to the hydroperoxo complex  $[\text{Cu}^{\text{II}}(\text{tepa})(\text{OOH})]^+$  (**3**) occurs, as shown by the data in Figure 11a, where the absorption spectrum due to **3** remained constant by the addition of Fc or  $\text{Me}_2\text{Fc}$ . This is the reason why the selective two-electron reduction of  $\text{O}_2$  by Fc and  $\text{Me}_2\text{Fc}$  occurs; that is, the hydroperoxo-copper(II) complex **3** is not susceptible to reduction, and thus with catalyst and  $\text{HClO}_4$ , protonation occurs instead and  $\text{H}_2\text{O}_2$  is produced.

When excess  $\text{HClO}_4$  was further added to an acetone solution of  $[\text{Cu}^{\text{II}}(\text{tepa})(\text{OOH})]^+$  (**3**) and  $\text{Me}_2\text{Fc}$ , the absorption band due to **3** disappeared without formation of  $\text{Me}_2\text{Fc}^+$  (Figure 11b), indicating that the protonation of **3** occurs to yield  $[\text{Cu}^{\text{II}}(\text{tepa})]^{2+}$  (**1**) and hydrogen peroxide; no reductive cleavage of peroxide occurs, even with the slightly stronger 1,1'-dimethylferrocene reductant.

We have also examined the temperature effect on this protonation step. Variable temperature studies revealed that the rate of protonation of  $[\text{Cu}^{\text{II}}(\text{tepa})(\text{OOH})]^+$  (**3**) became faster with increasing temperature (Figure S19 in SI). The second-order rate constant ( $k_2$ ) was estimated from Eyring plot to be  $(9.0 \pm 0.5) \times 10^2 \text{ M}^{-1} \text{ s}^{-1}$  at 298 K, which is much larger than the  $k_{\text{obs}}/[\mathbf{1}]$  values (vide supra). Thus, the protonation of hydroperoxo species is not the rate-determining step under the catalytic conditions.

The Eyring plot also afforded activation enthalpy ( $\Delta H^\ddagger = 8.4 \pm 0.2 \text{ kcal mol}^{-1}$ )<sup>57</sup> and activation entropy ( $\Delta S^\ddagger = -16 \pm 0.5 \text{ cal K}^{-1} \text{ mol}^{-1}$ ) parameters for the copper-hydroperoxide protonation step.



## Catalytic Mechanism

The catalytic mechanism of the two-electron reduction of O<sub>2</sub> by Me<sub>2</sub>Fc and Fc with [Cu<sup>II</sup>(tepa)]<sup>2+</sup> (**1**) in the presence of HClO<sub>4</sub> is summarized in Scheme 3. The initial electron transfer from Me<sub>2</sub>Fc and Fc to **1** is fast, followed by the reaction of the copper(I) complex formed, [Cu<sup>I</sup>(tepa)]<sup>+</sup> (**2**), with O<sub>2</sub> in the presence of HClO<sub>4</sub> to afford the hydroperoxo complex, [Cu<sup>II</sup>(tepa)(OOH)]<sup>+</sup> (**3**) via the formation of [Cu<sup>II</sup>(tepa)(O<sub>2</sub><sup>·-</sup>)]<sup>+</sup>, followed by PCET reduction. The fast direct protonation of **3** with HClO<sub>4</sub> rather than electron-transfer reduction of **3** by Me<sub>2</sub>Fc and Fc yields H<sub>2</sub>O<sub>2</sub>, accompanied by regeneration of **1**, leading to the overall catalytic two-electron reduction of O<sub>2</sub> by Me<sub>2</sub>Fc and Fc with HClO<sub>4</sub>. The O<sub>2</sub> binding step to [Cu<sup>I</sup>(tepa)]<sup>+</sup> combined with the PCET reduction of [Cu<sup>II</sup>(tepa)(O<sub>2</sub><sup>·-</sup>)] with HClO<sub>4</sub> is the rate limiting step in the overall catalytic reaction. The  $-\Delta H$  value of formation of [Cu<sup>II</sup>(tepa)(O<sub>2</sub><sup>·-</sup>)] is very close to being the same as the  $\Delta H$  value of the PCET reduction of [Cu<sup>II</sup>(tepa)(O<sub>2</sub><sup>·-</sup>)]<sup>+</sup>, resulting in unique temperature independent catalytic two-electron reduction of O<sub>2</sub> by weak one-electron reductants such as Me<sub>2</sub>Fc and Fc in the presence of HClO<sub>4</sub> in acetone.

## Conclusion

In summary, we have demonstrated that a subtle difference in ligand architecture, the addition of one -CH<sub>2</sub>- (methylene group) in the pyridylalkyl moiety of the ligand for Cu<sup>II</sup> in [Cu<sup>II</sup>(tepa)]<sup>2+</sup>, as compared with chemistry carried out with [Cu<sup>II</sup>(tmpa)]<sup>2+</sup>, results in the drastic change of the number of electrons reacting in the catalytic reduction of O<sub>2</sub>, a change from four for [Cu<sup>II</sup>(tmpa)]<sup>2+</sup> to two for [Cu<sup>II</sup>(tepa)]<sup>2+</sup>. The more positive one-electron reduction potential of [Cu<sup>II</sup>(tepa)]<sup>2+</sup>, in contrast to [Cu<sup>II</sup>(tmpa)]<sup>2+</sup>, has allowed us to employ relatively weak one-electron reductants, such as Fc and Me<sub>2</sub>Fc, differing from the case of [Cu<sup>II</sup>(tmpa)]<sup>2+</sup> which required the use of a strong one-electron reductant such as Fc\*. As a consequence, the rate-determining step changed from the electron-transfer reduction of [Cu<sup>II</sup>(tmpa)]<sup>2+</sup> to its copper(I) form, to PCET reduction of [Cu<sup>II</sup>(tepa)(O<sub>2</sub><sup>·-</sup>)]<sup>+</sup> to form [Cu<sup>II</sup>(tepa)(OOH)]<sup>+</sup>. This latter process exhibits no temperature dependence due to the cancellation of the heat of formation for the formation of [Cu<sup>II</sup>(tepa)(O<sub>2</sub><sup>·-</sup>)]<sup>+</sup> (a negative value) by the subsequent activation enthalpy for the PCET reduction (a positive value). It is also notable, that by use of perchloric acid to help drive the reaction toward Cu(II)-hydroperoxo formation, we have turned a copper(I) complex which is completely unreactive toward O<sub>2</sub>, to undergo oxygenation and facilitation of catalytic O<sub>2</sub>-reduction chemistry. This study has provided deeper insight into the control of two-electron vs four-electron reduction of O<sub>2</sub>, paving a promising way to the future development of efficient catalytic systems for production of H<sub>2</sub>O<sub>2</sub>, a promising candidate as a renewable energy source.<sup>58,59</sup>

## Supplementary Material

Refer to Web version on PubMed Central for supplementary material.

## Acknowledgments

This work was supported by Grants-in-Aid (Scientific Research on Innovative Areas Nos. 20108010 to S.F. and 23750014 to K.O.) by NRF/MEST of Korea through CRI (to W.N.), GRL (2010-00353) (to W.N.) and WCU (R31-2008-000-10010-0) (to W.N., S.F. and K.D.K.). K.D.K. also acknowledges support from the USA National Institutes of Health grant, GM28962.

## REFERENCES

- (1). (a) Holm RH, Kennepohl P, Solomon EI. *Chem. Rev.* 1996; 96:2239–2314. [PubMed: 11848828] (b) Klinman JP. *Chem. Rev.* 1996; 96:2541–2561. [PubMed: 11848836] (c) Mirica LM,

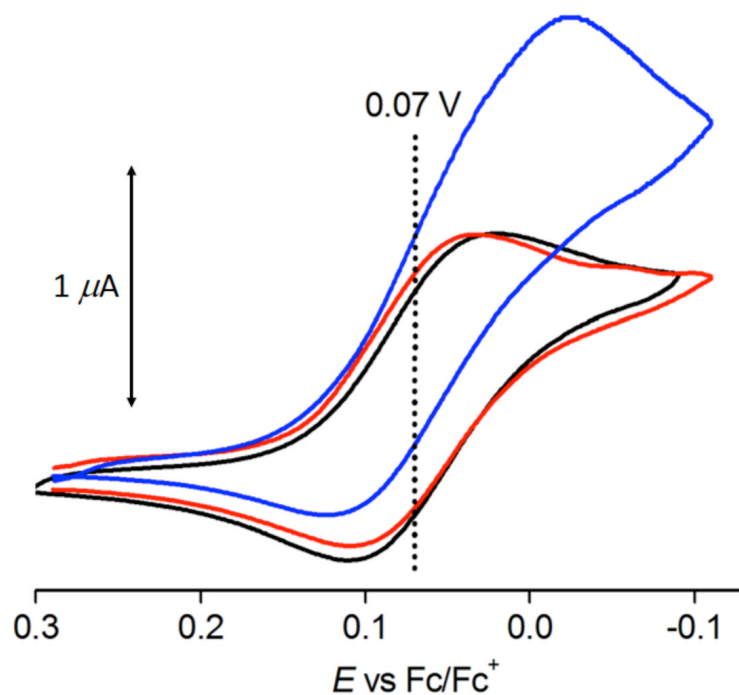
- Ottenwaelder X, Stack TDT. *Chem. Rev.* 2004; 104:1013–1046. [PubMed: 14871148] (d) Lewis EA, Tolman WB. *Chem. Rev.* 2004; 104:1047–1076. [PubMed: 14871149]
- (2). (a) Solomon EI, Ginsbach JW, Heppner DE, Kieber-Emmons MT, Kjaergaard CH, Smeets PJ, Tian L, Woertink JS. *Faraday Discuss.* 2011; 148:11–39. [PubMed: 21322475] (b) Solomon EI, Sundaram UM, Machonkin TE. *Chem. Rev.* 1996; 96:2563–2605. [PubMed: 11848837] (c) Solomon EI, Chen P, Metz M, Lee S-K, Palmer AE. *Angew. Chem., Int. Ed.* 2001; 40:4570–4590. (d) Karlin, KD.; Tyeklár, Z., editors. *Bioinorganic Chemistry of Copper*. Chapman & Hall; New York: 1993. (e) Karlin, KD.; Zuberbühler, AD. *Formation, Structure and Reactivity of Copper Dioxide Complexes*. In: Reedijk, J.; Bouwman, E., editors. *Bioinorganic Catalysis*. 2nd ed.. Marcel Dekker, Inc.; New York: 1999. p. 469-534. (f) Quant Hatcher L, Karlin KD. *J. Biol. Inorg. Chem.* 2004; 9:669–683. [PubMed: 15311336] (g) Lee, Y.; Karlin, KD. *Highlights of Copper Protein Active-Site Structure/Reactivity and Synthetic Model Studies*. In: Metzler-Nolte, N.; Kraatz, H-B., editors. *Concepts and Models in Bioinorganic Chemistry*. Wiley-VCH; New York: 2006. p. 363-395.
- (3). (a) Karlin KD. *Science.* 1993; 261:701–708. [PubMed: 7688141] (b) Metzler-Nolte, N.; Kraatz, H-B. *Concepts and Models in Bioinorganic Chemistry*. Wiley-VCH; New York: 2006.
- (4). (a) Klinman JP. *J. Biol. Chem.* 2006; 281:3013–3016. [PubMed: 16301310] (b) Prigge ST, Eipper B, Mains R, Amzel LM. *Science.* 2004; 304:864–867. [PubMed: 15131304] (c) Chen P, Solomon EI. *Proc. Natl. Acad. Sci. U.S.A.* 2004; 101:13105–13110. [PubMed: 15340147] (d) Balasubramanian R, Smith SM, Rawat S, Yatsunyk LA, Stemmler TL, Rosenzweig AC. *Nature.* 2010; 465:115–119. [PubMed: 20410881] (e) Chan SI, Yu SS-F. *Acc. Chem. Res.* 2008; 41:969–979. [PubMed: 18605740]
- (5). Humphreys KJ, Mirica LM, Wang Y, Klinman JP. *J. Am. Chem. Soc.* 2009; 131:4657–4663. [PubMed: 19290629]
- (6). Mukherjee A, Smirnov VV, Lanci MP, Brown DE, Shepard EM, Dooley DM, Roth JP. *J. Am. Chem. Soc.* 2008; 130:9459–9473. [PubMed: 18582059]
- (7). McGuirl, MA.; Dooley, DM. *Copper Proteins with Type 2 Sites*. In: King, RB., editor. *Encyclopedia of Inorganic Chemistry*. 2nd ed.. Vol. II. John Wiley & Sons Ltd.; Chichester: 2005. p. 1201-1225.
- (8). (a) Blanford CF, Heath RS, Armstrong FA. *Chem. Commun.* 2007:1710. (b) Mano N, Soukharev V, Heller A. *J. Phys. Chem. B.* 2006; 110:11180–11187. [PubMed: 16771381]
- (9). (a) Ferguson-Miller S, Babcock GT. *Chem. Rev.* 1996; 96:2889–2908. [PubMed: 11848844] (b) Pereira MM, Santana M, Teixeira M. *Biochim. Biophys. Acta.* 2001; 1505:185–208. [PubMed: 11334784]
- (10). (a) Tsukihara T, Aoyama H, Yamashita E, Tomizaki T, Yamaguchi H, Shinzawa-Itoh K, Nakashima R, Yaono R, Yoshikawa S. *Science.* 1995; 269:1069–1074. [PubMed: 7652554] (b) Yoshikawa S, Shinzawa-Itoh K, Nakashima R, Yaono R, Yamashita E, Inoue N, Yao M, Fei MJ, Libeu CP, Mizushima T, Yamaguchi H, Tomizaki T, Tsukihara T. *Science.* 1998; 280:1723–1729. [PubMed: 9624044]
- (11). (a) Collman JP, Devaraj NK, Decreau RA, Yang Y, Yan Y-L, Ebina W, Eberspacher TA, Chidsey CED. *Science.* 2007; 315:1565–1568. [PubMed: 17363671] (b) Collman JP, Decréau RA, Lin H, Hosseini A, Yang Y, Dey A, Eberspacher TA. *Proc. Natl. Acad. Sci. U.S.A.* 2009; 106:7320–7323. [PubMed: 19380725] (c) Collman JP, Ghosh S, Dey A, Decréau RA, Yang Y. *J. Am. Chem. Soc.* 2009; 131:5034–5035. [PubMed: 19317484]
- (12). Kadish KM, Frémond L, Shen J, Chen P, Ohkubo K, Fukuzumi S, El Ojaimi M, Gros CP, Barbe J-M, Guillard R. *Inorg. Chem.* 2009; 48:2571–2582. [PubMed: 19215120]
- (13). (a) Hatay I, Su B, Li F, Méndez MA, Khoury T, Gros CP, Barbe J-M, Ersoz M, Samec Z, Girault HH. *J. Am. Chem. Soc.* 2009; 131:13453–13459. [PubMed: 19715275] (b) Partovi-Nia R, Su B, Li F, Gros CP, Barbe J-M, Samec Z, Girault HH. *Chem.-Eur. J.* 2009; 15:2335–2340. [PubMed: 19156806] (c) Hatay I, Su B, Méndez MA, Corminboeuf C, Khoury T, Gros CP, Bourdillon M, Meyer M, Barbe J-M, Ersoz M, Zális S, Samec Z, Girault HH. *J. Am. Chem. Soc.* 2010; 132:13733–13741. [PubMed: 20828124]
- (14). (a) Partovi-Nia R, Su B, Méndez MA, Habermeyer B, Gros CP, Barbe J-M, Samec Z, Girault HH. *ChemPhysChem.* 2010; 11:2979–2984. [PubMed: 20607710] (b) Su B, Hatay I, Trojáněk A,

- Samec Z, Khoury T, Gros CP, Barbe J-M, Daina A, Carrupt P-A, Girault HH. *J. Am. Chem. Soc.* 2010; 132:2655–2662. [PubMed: 20131825]
- (15). Zagal JH, Griveau S, Silva JF, Nyokong T, Bedioui F. *Coord. Chem. Rev.* 2010; 254:2755–2791.
- (16). Cracknell JA, Vincent KA, Armstrong FA. *Chem. Rev.* 2008; 108:2439–2461. [PubMed: 18620369]
- (17). (a) Thorum MS, Yadav J, Gewirth AA. *Angew. Chem., Int. Ed.* 2009; 48:165–167. (b) Thorseth MA, Letko CS, Rauchfuss TB, Gewirth AA. *Inorg. Chem.* 2011; 50:6158–6162. [PubMed: 21627090] (c) McCrory CCL, Devadoss A, Ottenwaelder X, Lowe RD, Stack TDP, Chidsey CED. *J. Am. Chem. Soc.* 2011; 133:3696–3699. [PubMed: 21366244] (d) Thorseth MA, Tornow CE, Tse ECM, Gewirth AA. *Coord. Chem. Rev.* 2013; 257:130–139.
- (18). (a) Stambouli AB, Traversa E. *Renew. Sust. Energy Rev.* 2002; 6:295–304. (b) Markovi NM, Schmidt TJ, Stamenkovi V, Ross PN. *Fuel Cells.* 2001; 1:105–116. (c) Steele BCH, Heinzl A. *Nature.* 2001; 414:345–352. [PubMed: 11713541]
- (19). Borup R, Meyers J, Pivovar B, Kim YS, Mukundan R, Garland N, Myers D, Wilson M, Garzon F, Wood D, Zelenay P, More K, Stroh K, Zawodzinski T, Boncella J, McGrath JE, Inaba M, Miyatake K, Hori M, Ota K, Ogumi Z, Miyata S, Nishikata A, Siroma Z, Uchimoto Y, Yasuda K, Kimijima K.-i, Iwashita N. *Chem. Rev.* 2007; 107:3904–3951. [PubMed: 17850115]
- (20). (a) Lee, K.; Zhang, L.; Zhang, J. *PEM Fuel Cell Electrocatalysts and Catalyst Layers.* Springer; London: 2008. p. 715 (b) Anson FC, Shi C, Steiger B. *Acc. Chem. Res.* 1997; 30:437–444. (c) Wang B. *J. Power Sources.* 2005:152. (d) Peljo P, Rauhala T, Murtomäki L, Kallio T, Kontturi K. *Int. J. Hydrogen Energy.* 2011; 36:10033–10043.
- (21). (a) Collman JP, Devaraj NK, Decréau RA; Yang Y, Yan Y-L, Ebina W, Eberspacher TA; Chidsey CED. *Science.* 2007; 315:1565–1568. [PubMed: 17363671] (b) Collman JP, Decréau RA, Lin H, Hosseini A, Yang Y, Dey A, Eberspacher TA. *Proc. Natl. Acad. Sci. U.S.A.* 2009; 106:7320–7323. [PubMed: 19380725] (c) Collman JP, Ghosh S, Dey A, Decréau RA, Yang Y. *J. Am. Chem. Soc.* 2009; 131:5034–5035. [PubMed: 19317484]
- (22). (a) Kadish KM, Shen J, Frémond L, Chen P, Ojaimi ME, Chkounda M, Gros CP, Barbe J-M, Ohkubo K, Fukuzumi S, Guillard R. *Inorg. Chem.* 2008; 47:6726–6737. [PubMed: 18582035] (b) Chen W, Akhigbe J, Brückner C, Li CM, Lei Y. *J. Phys. Chem. C.* 2010; 114:8633–8645.
- (23). (a) Rosenthal J, Nocera DG. *Acc. Chem. Res.* 2007; 40:543–553. [PubMed: 17595052] (b) Chang CJ, Loh Z-H, Shi C, Anson FC, Nocera DG. *J. Am. Chem. Soc.* 2004; 126:10013–10020. [PubMed: 15303875] (c) Dogutan DK, Stoian SA; McGuire R, Schwalbe M, Teets TS, Nocera DG. *J. Am. Chem. Soc.* 2011; 133:131–140. [PubMed: 21142043] (d) Teets TS, Cook TR, McCarthy BD, Nocera DG. *J. Am. Chem. Soc.* 2011; 133:8114–8117. [PubMed: 21539366]
- (24). (a) Fukuzumi S, Kotani H, Lucas HR, Doi K, Suenobu T, Peterson RL, Karlin KD. *J. Am. Chem. Soc.* 2010; 132:6874–6875. [PubMed: 20443560] (b) Tahsini L, Kotani H, Lee Y-M, Cho J, Nam W, Karlin KD, Fukuzumi S. *Chem.-Eur. J.* 2012; 18:1084–1093. [PubMed: 22237962]
- (25). Halime Z, Kotani H, Li Y, Fukuzumi S, Karlin KD. *Proc. Natl. Acad. Sci. U.S.A.* 2011; 108:13990–13994. [PubMed: 21808032]
- (26). Fukuzumi S, Tahsini L, Lee Y-M, Ohkubo K, Nam W, Karlin KD. *J. Am. Chem. Soc.* 2012; 134:7025–7035. [PubMed: 22462521]
- (27). (a) Yamada Y, Fukunishi Y, Yamazaki S.-i, Fukuzumi S. *Chem. Commun.* 2010; 46:7334–7336. (b) Jing X, Cao DX, Liu Y, Wang GL, Yin JL, Wen Q, Gao YYJ. *Electroanal. Chem.* 2011; 658:46–51.
- (28). (a) Lei T, Tian YM, Wang GL, Yin JL, Gao YY, Wen Q, Cao DX. *Fuel Cells.* 2011; 11:431–435. (b) Hasvold O, Storkersen NJ, Forseth S, Lian TJ. *Power Sources.* 2006; 162:935–942. (c) Patrissi CJ, Bessette RR, Kim YK, Schumacher CR. *J. Electrochem. Soc.* 2008; 155:B558–B562.
- (29). (a) Disselkamp RS. *Energy Fuels.* 2008; 22:2771–2774. (b) Disselkamp RS. *Int. J. Hydrogen Energy.* 2010; 35:1049–1053.
- (30). Galbács ZM, Csányi LJ. *J. Chem. Soc., Dalton Trans.* 1983:2353–2357.
- (31). Latimer, WM. *The Oxidation States of the Elements and their Potentials in Aqueous Solutions.* Prentice-Hall; New York: 1952. p. 39
- (32). (a) Abrantes S, Amaral E, Costa AP, Shatalov AA, Duarte AP. *Ind. Crop. Prod.* 2007; 25:288–293. (b) Zeronian SH, Inglesby MK. *Cellulose.* 1995; 2:265–272.

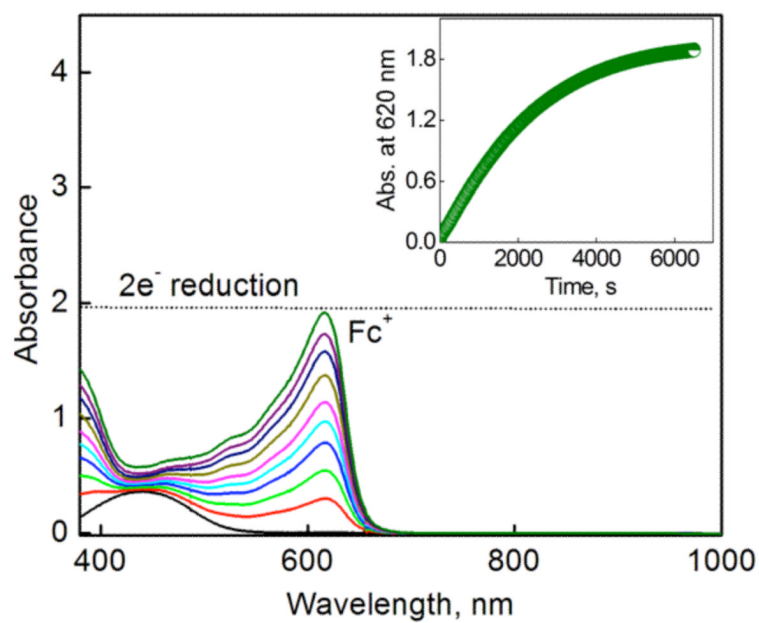
- (33). Li L, Lee S, Lee HL, Youn HJ. *BioResources*. 2011; 6:721–736.
- (34). (a) Schatz M, Becker M, Thaler F, Hampel F, Schindler S, Jacobson RR, Tyeklár Z, Murthy NN, Ghosh P, Chen Q, Zubieta J, Karlin KD. *Inorg. Chem.* 2001; 40:2312–2322. [PubMed: 11327908] (b) Wei N, Murthy NN, Karlin KD. *Inorg. Chem.* 1994; 33:6093–6100.
- (35). Armarego, WLF.; Chai, CLL. *Purification of Laboratory Chemicals*. 5th ed.. Butterworth-Heinemann; Amsterdam: 2003.
- (36). Baek HK, Karlin KD, Holwerda RA. *Inorg. Chem.* 1986; 25:2347–2349.
- (37). Fukuzumi S, Ishikawa M, Tanaka T. *J. Chem. Soc., Perkin Trans.* 1989; 2:1037–1045.
- (38). (a) Mair RD, Graupner A. *J. Anal. Chem.* 1964; 36:194–203. (b) Fukuzumi S, Kuroda S, Tanaka T. *J. Am. Chem. Soc.* 1985; 107:3020–3027.
- (39). (a) Karlin KD, Hayes JC, Juen S, Hutchinson JP, Zubieta J. *Inorg. Chem.* 1982; 21:4106–4108. (b) Karlin KD, Sherman SE. *Inorg. Chim. Acta.* 1982; 65:L39–L40. (c) Ambundo EA, Deydier M-V, Grall AJ, Aguera-Vega N, Dressel LT, Cooper TH, Heeg MJ, Ochrymowycz LA, Rorabacher DB. *Inorg. Chem.* 1999; 38:4233–4242. (d) Rorabacher DB. *Chem. Rev.* 2004; 104:651–697. [PubMed: 14871138]
- (40). (a) Lee Y-M, Kotani H, Suenobu T, Nam W, Fukuzumi S. *J. Am. Chem. Soc.* 2008; 130:434–435. [PubMed: 18085783] (b) Fukuzumi S, Kotani H, Prokop KA, Goldberg DP. *J. Am. Chem. Soc.* 2011; 133:1859–1869. [PubMed: 21218824] (c) Fukuzumi S, Kotani H, Suenobu T, Hong S, Lee Y-M, Nam W. *Chem.-Eur. J.* 2010; 16:354–361. [PubMed: 19937616] (d) Comba P, Fukuzumi S, Kotani H, Wunderlich S. *Angew. Chem., Int. Ed.* 2010; 49:2622–2625.
- (41). The  $E_{ox}$  values of ferrocene derivatives in acetone are virtually the same as those in MeCN; see: Noviadri I, Brown KN, Fleming DS, Gulyas PT, Lay PA, Masters AF, Phillips L. *J. Phys. Chem. B.* 1999; 103:6713–6722.
- (42). The activation entropy for electron transfer becomes negative when the electron transfer occurs via an intermediate, see: Fukuzumi S, Endo Y, Imahori H. *J. Am. Chem. Soc.* 2002; 124:10974–10975. [PubMed: 12224933]
- (43). Fujii T, Naito A, Yamaguchi S, Wada A, Funahashi Y, Jitsukawa K, Nagatomo S, Kitagawa T, Masuda H. *Chem. Commun.* 2003:2700–2701.
- (44). Wada A, Harata M, Hasegawa K, Jitsukawa K, Masuda H, Mukai M, Kitagawa T, Einaga H. *Angew. Chem. Int. Ed.* 1998; 37:798–800.
- (45). Kodera M, Kita T, Miura I, Nakayama N, Kawata T, Kano K, Hirota S. *J. Am. Chem. Soc.* 2001; 123:7715–7716. [PubMed: 11481001]
- (46). (a) Karlin KD, Cruse RW, Gultneh Y. *J. Chem. Soc., Chem. Commun.* 1987:599–600. (b) Karlin KD, Ghosh P, Cruse RW, Farooq A, Gultneh Y, Jacobson RR, Blackburn NJ, Strange RW, Zubieta J. *J. Am. Chem. Soc.* 1988; 110:6769–6780. (c) Root DE, Mahroof-Tahir M, Karlin KD, Solomon EI. *Inorg. Chem.* 1998; 37:4838–4848. [PubMed: 11670647]
- (47). Kunishita A, Kubo M, Ishimaru H, Ogura T, Sugimoto H, Itoh S. *Inorg. Chem.* 2008; 47:12032–12039. [PubMed: 18998628]
- (48). In the case of  $[Cu(tepa)]^{2+}$ ,  $g_{xx} = g_{yy}$  with the same broad linewidth ( $\sigma_{xx} = \sigma_{yy} = 100$  G). In such a case no superhyperfine due to nitrogens was detected. In the case of  $[Cu^{II}(tepa)OOH]^+$ , however, the linewidth of  $\sigma_{xx}$  (10 G) is much smaller than  $\sigma_{yy}$  (70 G) although  $g_{xx} = g_{yy}$ . This is the reason why the superhyperfine due to nitrogens was detected for  $[Cu^{II}(tepa)OOH]^+$  in Figures 8b and 8c.
- (49). Alilou EH, Hallaoui AE, Ghadraoui EHE, Giorgi M, Pierrot M, Réglie M. *Acta Cryst. Section C.* 1997; C53:559–562.
- (50). Karlin KD, Hayes JC, Hutchinson JP, Hyde JR, Zubieta J. *Inorg. Chim. Acta.* 1982; 64:L219–L220.
- (51). Karlin KD, Wei N, Jung B, Kaderli S, Niklaus P, Zuberbühler AD. *J. Am. Chem. Soc.* 1993; 115:9506–9514.
- (52). Karlin KD, Kaderli S, Zuberbühler AD. *Acc. Chem. Res.* 1997; 30:139–147.
- (53). (a) Fukuzumi S, Endo Y, Imahori H. *J. Am. Chem. Soc.* 2002; 124:10974–10975. [PubMed: 12224933] (b) Yoder JC, Roth JP, Gussenhoven EM, Larsen AS, Mayer JM. *J. Am. Chem. Soc.* 2003; 125:2629–2640. [PubMed: 12603151]

- (54). (a) Zaman KM, Yamamoto S, Nishimura N, Maruta J, Fukuzumi S. *J. Am. Chem. Soc.* 1994; 116:12099–12100. (b) Fukuzumi S, Ohkubo K, Tokuda Y, Suenobu T. *J. Am. Chem. Soc.* 2000; 122:4286–4294. (c) Zhu X-Q, Zhang J-Y, Cheng J-P. *J. Org. Chem.* 2006; 71:7007–7015. [PubMed: 16930056]
- (55). Ohkubo K, Fukuzumi S. *J. Phys. Chem. A.* 2005; 109:1105–1113. [PubMed: 16833419]
- (56). Zhang CX, Kaderli S, Costas M, Kim E.-i, Neuhold Y-M, Karlin KD, Zuberbuhler AD. *Inorg. Chem.* 2003; 42:1807–1824. [PubMed: 12639113]
- (57). Because the overall catalytic reaction has no temperature dependence, the  $\Delta H$  value may be smaller than the  $-\Delta H$  value of formation of the hydroperoxo complex in Scheme 2.
- (58). Fukuzumi S, Yamada Y, Karlin KD. *Electrochim. Acta.* 2012; 82:493–511. [PubMed: 23457415]
- (59). (a) Yamada Y, Yoshida S, Honda T, Fukuzumi S. *Energy Environ. Sci.* 2011; 4:2822–2825. (b) Shaegh SAM, Nguyen N-T, Ehteshami SMM, Chan SH. *Energy Environ. Sci.* 2012; 5:8225–8228.

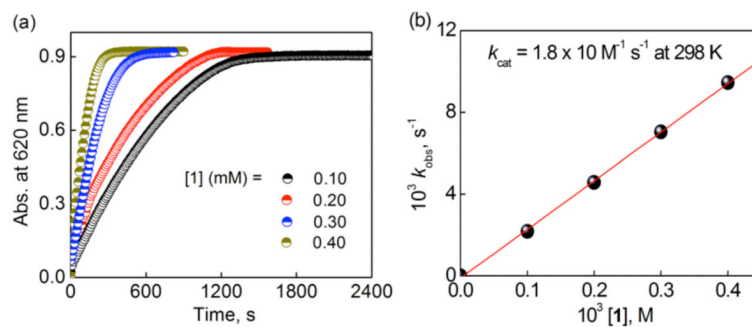




**Figure 1.** Cyclic voltammograms of **1** (1.0 mM) in deaerated (black line) and  $O_2$ -saturated (red line) acetone in the absence of  $HClO_4$  and in the presence of  $HClO_4$  (0.10 M) in  $O_2$ -saturated acetone (blue line) at 298 K. Working and counter electrodes were a glassy carbon electrode and a Pt wire, respectively.  $TBAPF_6$  (0.10 M) was used as an electrolyte. Sweep rate was  $1.0 \text{ mV s}^{-1}$ .



**Figure 2.** UV-vis spectral changes observed in the two-electron reduction of O<sub>2</sub> (2.2 mM) by Fc (10 mM) with HClO<sub>4</sub> (40 mM) catalyzed by **1** (0.040 mM) in acetone at 298 K. The inset shows the time profile of the absorbance at 620 nm due to Fc<sup>+</sup>.

**Figure 3.**

(a) Time profiles of the absorbance at 620 nm due to  $\text{Fc}^+$  in the two-electron reduction of  $\text{O}_2$  ( $[\text{O}_2] = 1.0 \text{ mM}$ ) catalyzed by **1** (0.10 mM (black), 0.20 mM (red), 0.30 mM (blue), and 0.40 mM (dark yellow)) with  $\text{Fc}$  (10 mM) in the presence of  $\text{HClO}_4$  (60 mM) in acetone solution at 298 K. (b) Plot of  $k_{\text{obs}}$  versus  $[\mathbf{1}]$  for the two-electron reduction of  $\text{O}_2$  ( $[\text{O}_2] = 1.0 \text{ mM}$ ) catalyzed by **1** with  $\text{Fc}$  (10 mM) in the presence of  $\text{HClO}_4$  (60 mM) in acetone at 298 K.

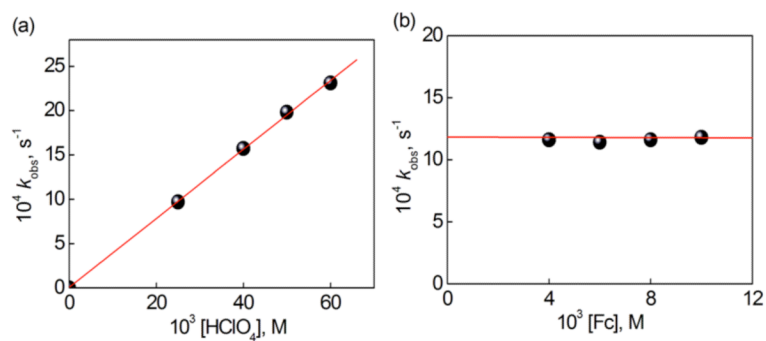


**Figure 4.**

(a) Plot of  $k_{\text{obs}}$  versus  $[\text{HClO}_4]$  for the two-electron reduction of  $\text{O}_2$  by Fc (10 mM) catalyzed by **1** (0.10 mM) in an acetone solution containing  $\text{O}_2$  (1.0 mM) at 298 K. (b) Plot of  $k_{\text{obs}}$  versus  $[\text{Fc}]$  for the two-electron reduction of  $\text{O}_2$  catalyzed by **1** (0.10 mM) with Fc in the presence of  $\text{HClO}_4$  (30 mM) in an acetone solution containing  $\text{O}_2$  ( $[\text{O}_2] = 1.0$  mM) at 298 K.

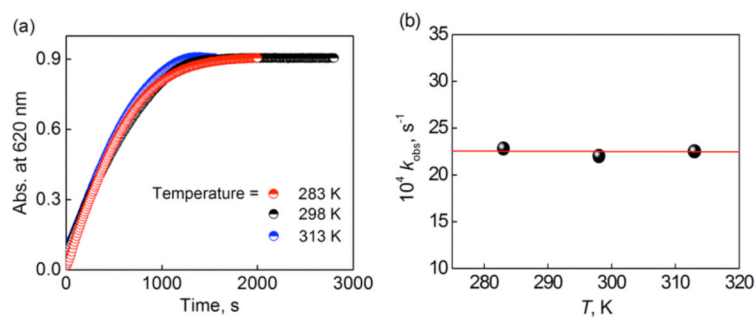


**Figure 5.**

(a) Time profiles of the absorbance at 620 nm due to  $\text{Fc}^+$  in the two-electron reduction of  $\text{O}_2$  (1.0 mM) catalyzed by **1** (0.10 mM) with Fc (10 mM) in the presence of  $\text{HClO}_4$  (60 mM) in an acetone solution at variable temperatures (283 K (red), 298 K (black) and 313 K (blue)).

(b) Plot of  $k_{\text{obs}}$  versus temperature ( $T$ ) for the two-electron reduction of  $\text{O}_2$  catalyzed by **1** (0.10 mM) with Fc (10 mM) in the presence of  $\text{HClO}_4$  (60 mM) in an acetone solution with  $\text{O}_2$  ( $[\text{O}_2] = 1.0 \text{ mM}$ ) at different temperatures.



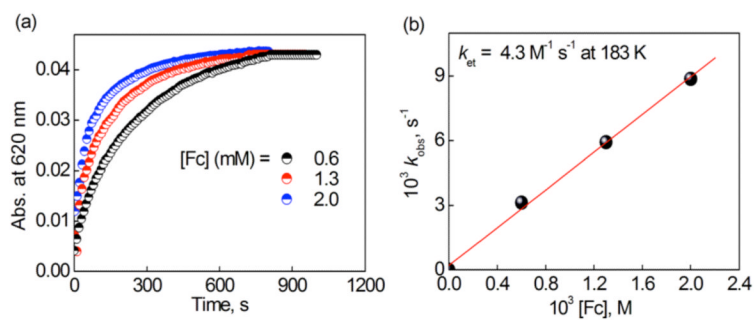


**Figure 6.**

(a) Time profiles of the absorbance at 620 nm due to  $\text{Fc}^+$  in the electron transfer reaction from Fc (0.60 mM (black), 1.3 mM (red) and 2.0 mM (blue)) to **1** (0.10 mM) in acetone at 183 K and (b) Plot of  $k_{\text{obs}}$  versus  $[\text{Fc}]$  in the electron transfer from Fc to  $[\text{Cu}^{\text{II}}(\text{tepa})]^{2+}$  (**1**) (0.10 mM) in an acetone solution at 183 K.

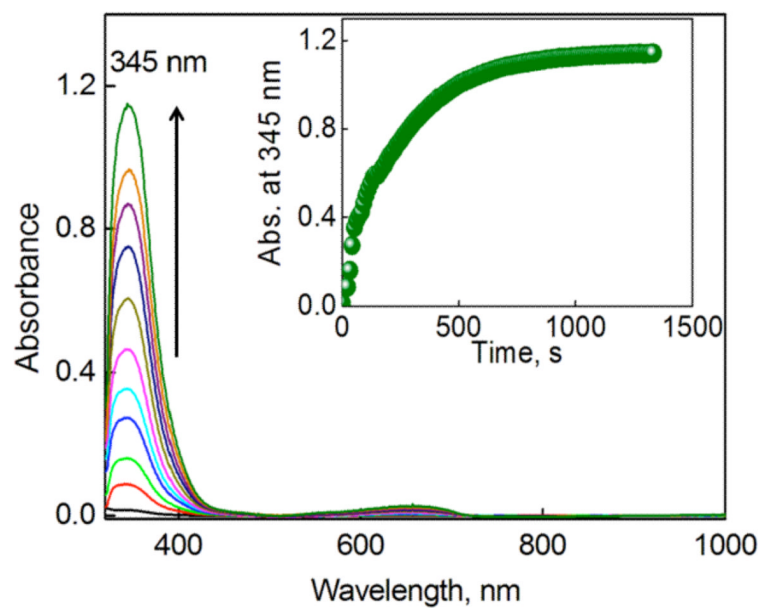


**Figure 7.**

Formation of the hydroperoxo complex,  $[\text{Cu}^{\text{II}}(\text{tepa})(\text{OOH})]^+$  (**3**) ( $\lambda_{\text{max}} = 345 \text{ nm}$ ) in the reaction of  $[\text{Cu}^{\text{I}}(\text{tepa})]^+$  (0.16 mM)  $\{[\text{Cu}^{\text{I}}(\text{tepa})]^+$  was generated from room temperature mixing of  $[\text{Cu}^{\text{II}}(\text{tepa})]^{2+}$  (0.16 mM) with Fc (0.32 mM)  $\}$  with  $\text{O}_2$  (2.2 mM) in acetone at 193 K in the presence of  $\text{HClO}_4$  (3.0 mM). The inset shows the time profile of the absorbance at 345 nm due to the generation of  $[\text{Cu}^{\text{II}}(\text{tepa})(\text{OOH})]^+$  (**3**).

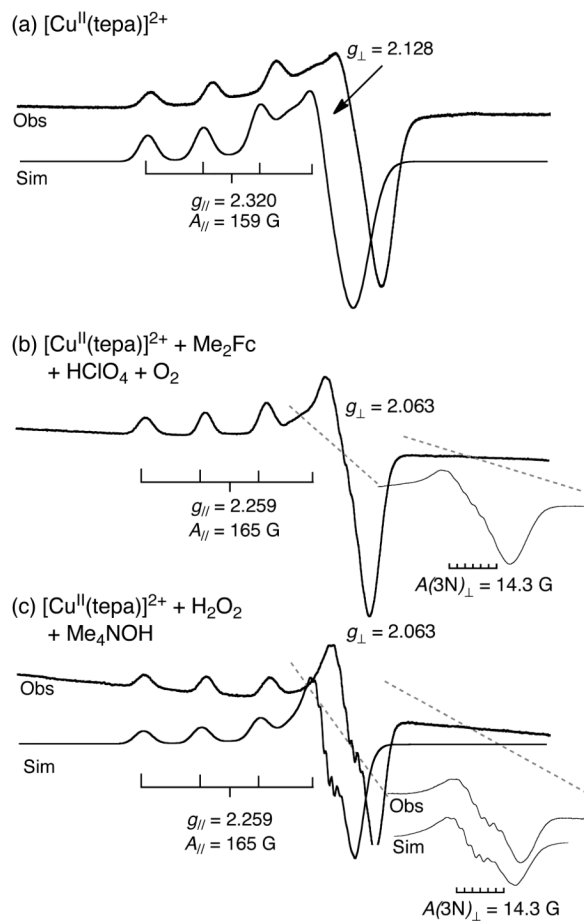


**Figure 8.**

X-band EPR spectra of (a)  $[\text{Cu}^{\text{II}}(\text{tepa})]^{2+}$  ( $5.0 \times 10^{-5}$  M) in deaerated acetone at 77 K, (b) the reaction solution of **1** ( $5.0 \times 10^{-5}$  M) with  $\text{Me}_2\text{Fc}$  ( $3.0 \times 10^{-4}$  M) in the presence of  $\text{HClO}_4$  ( $3.0 \times 10^{-3}$  M) in  $\text{O}_2$ -saturated acetone at 77 K and (c)  $[\text{Cu}^{\text{II}}(\text{tepa})(\text{OOH})]^+$  (**3**) generated by reaction of  $[\text{Cu}^{\text{II}}(\text{tepa})]^{2+}$  ( $5.0 \times 10^{-5}$  M) with  $\text{H}_2\text{O}_2$  ( $1.0 \times 10^{-3}$  M) in presence of  $\text{Me}_4\text{NOH}$  ( $1.0 \times 10^{-3}$  M) recorded in deaerated acetone at 77 K. The experimental parameters: microwave frequency = 9.2 GHz, microwave power = 1.0 mW and modulation frequency = 100 kHz. The simulated spectra were obtained with the EPR parameters of  $g_{\parallel} = 2.320$ ,  $g_{\perp} = 2.128$ ,  $A_{\parallel} = 159$  G,  $A_{\perp} = 25$  G, linewidth  $\sigma_{\parallel}$  ( $\sigma_{zz}$ ) = 48 G,  $\sigma_{\perp} = \sigma_{xx} = \sigma_{yy} = 100$  G for  $[\text{Cu}^{\text{II}}(\text{tepa})]^{2+}$  and  $g_{\parallel} = 2.259$ ,  $g_{\perp} = 2.063$ ,  $A_{\parallel} = 165$  G,  $A_{\perp} = 22$  G, linewidth  $\sigma_{\parallel}$  ( $\sigma_{zz}$ ) = 25 G,  $\sigma_{xx} = 10$  and  $\sigma_{yy} = 70$  G for Cu and 14.3 G for 3N of  $[\text{Cu}^{\text{II}}(\text{tepa})(\text{OOH})]^+$ .

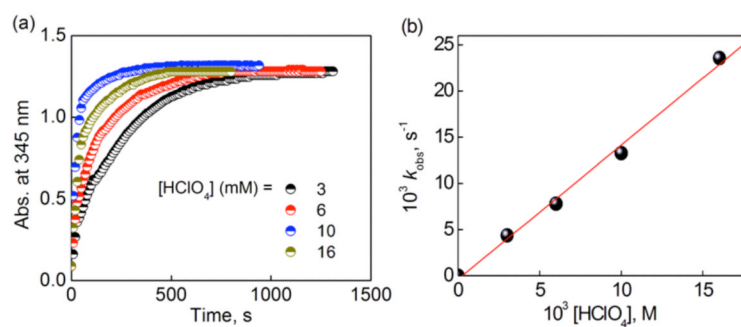


**Figure 9.**

(a) Time profiles of the absorbance at 345 nm due to  $[\text{Cu}^{\text{II}}(\text{tepa})(\text{OOH})]^+$  (**3**) in the  $\text{O}_2$  (2.2 mM) binding step to  $[\text{Cu}^{\text{I}}(\text{tepa})]^+$  (0.18 mM) ( $[\text{Cu}^{\text{I}}(\text{tepa})]^+$  was produced from room temperature mixing of  $[\text{Cu}^{\text{II}}(\text{tepa})]^{2+}$  (0.18 mM) with Fc (0.36 mM)) in the presence of various concentrations of  $\text{HClO}_4$  (3 mM (black), 6 mM (red), 10 mM (blue) and 16 mM (dark yellow)) in an acetone solution at 193 K. (b) Plot of  $k_{\text{obs}}$  versus  $[\text{HClO}_4]$  for the  $\text{O}_2$  (2.2 mM) binding step to  $[\text{Cu}^{\text{I}}(\text{tepa})]^+$  (0.18 mM) in the presence of various concentrations of  $\text{HClO}_4$ .

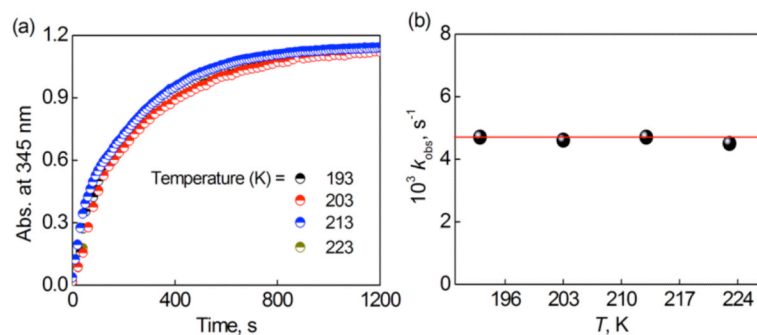


**Figure 10.**

(a) Time profiles of the absorbance at 345 nm due to  $[\text{Cu}^{\text{II}}(\text{tepa})(\text{OOH})]^+$  in the  $\text{O}_2$  ( $[\text{O}_2] = 2.2 \text{ mM}$ ) binding step in the presence of  $\text{HClO}_4$  (3.0 mM) with  $[\text{Cu}^{\text{I}}(\text{tepa})]^+$  (0.16 mM) ( $[\text{Cu}^{\text{I}}(\text{tepa})]^+$  was produced from room temperature mixing of  $[\text{Cu}^{\text{II}}(\text{tepa})]^{2+}$  (0.16 mM) with Fc (0.32 mM)) at different temperatures (193 K (black), 203 K (red), 213 K (blue) and 223 K (dark yellow)). (b) Plot of  $k_{\text{obs}}$  versus  $T$  (K) in the  $\text{O}_2$  (2.2 mM) binding process to  $[\text{Cu}^{\text{I}}(\text{tepa})]^+$  (2) (0.16 mM) with  $\text{HClO}_4$  (3.0 mM) in an acetone solution at variable temperatures.



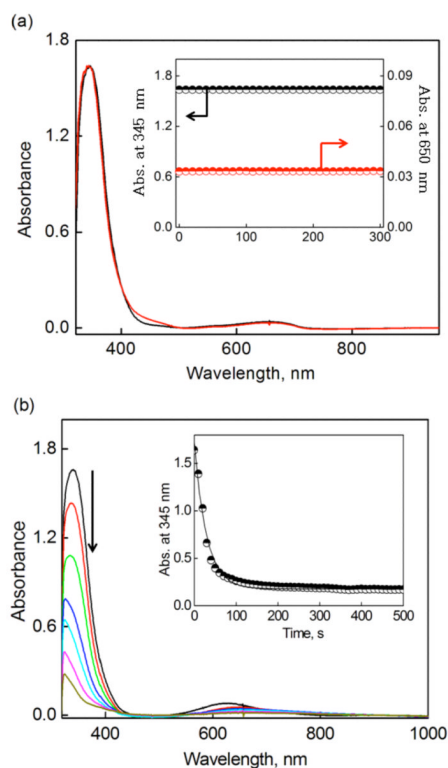
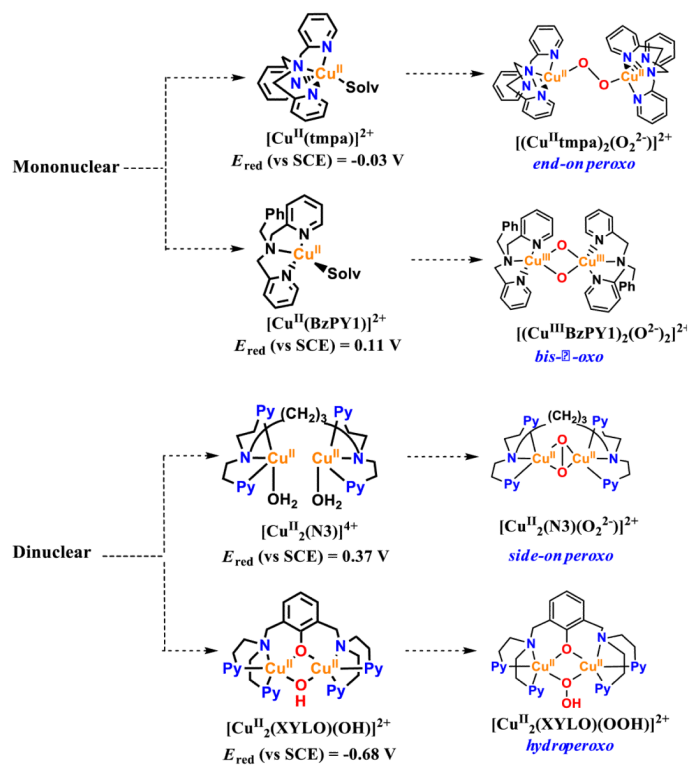
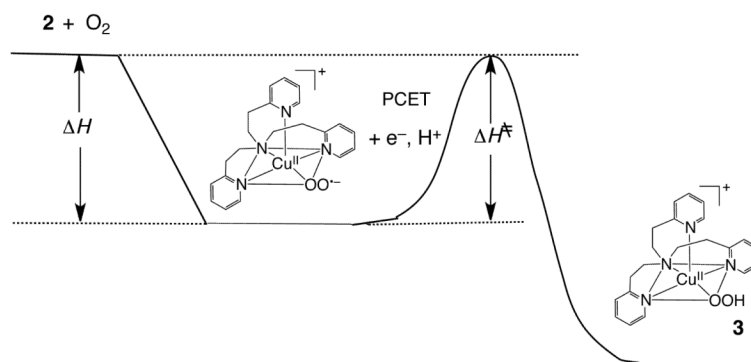


**Figure 11.**

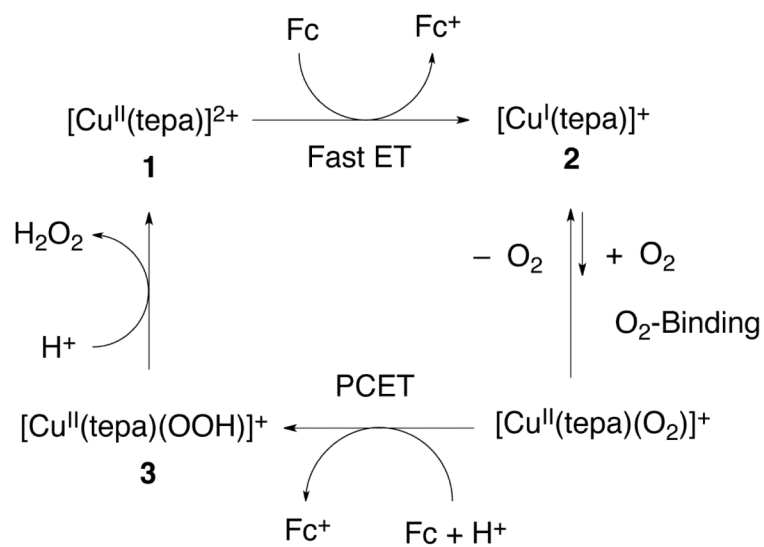
(a) UV-visible spectra of the hydroperoxo species  $[\text{Cu}^{\text{II}}(\text{tepa})(\text{OOH})^+$  (**3**) (0.23 mM) (black line) and **3** (0.23 mM) plus excess  $\text{Me}_2\text{Fc}$  (1.5 mM) (red line) in acetone at 193 K. (b) UV-visible spectral changes of **3** (0.23 mM) in the presence of  $\text{HClO}_4$  (40 mM) in acetone at 193 K. Inset shows the time profile of the absorbance at 345 nm due to **3**.



Scheme 1.



Scheme 2.



Scheme 3.

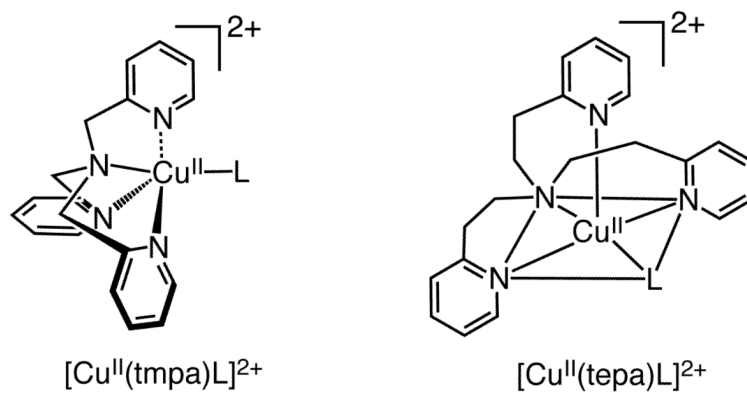


Chart 1.